


Article

The Elasticity of the Neutron Star Mantle: The Improved Compressible Liquid Drop Model for Cylindrical Phases

Nikita A. Zemlyakov and Andrey I. Chugunov * 

Ioffe Institute, 26 Politekhnikeskaya St., 194021 St. Petersburg, Russia; zemlyakov@mail.ioffe.ru

* Correspondence: andr.astro@mail.ioffe.ru

Abstract: Neutron stars are the densest objects in the Universe. They have a microscopically homogeneous core and heterogeneous crust. In particular, there may be a specific layer inside neutron stars, the mantle, which consists of substantially non-spherical nuclei immersed in a background of relativistic degenerate electrons and quasi-free neutrons. In this paper, we reconsider the transverse shear modulus for cylindrical phases of the mantle within the framework of the compressible liquid drop model. We demonstrate that transverse shearing affects the shape of nuclear clusters: their cross-section becomes elliptical. This effect reduces the respective elastic constant. Using a simple model, we perform all derivations analytically and obtain the expression for the transverse shear modulus, which can be useful for astrophysical applications.

Keywords: neutron stars; dense matter; elastic properties; pasta phase



Citation: Zemlyakov, N.A.; Chugunov, A.I. The Elasticity of the Neutron Star Mantle: The Improved Compressible Liquid Drop Model for Cylindrical Phases. *Universe* **2023**, *9*, 220. <https://doi.org/10.3390/universe9050220>

Academic Editor: Xinyu Li

Received: 29 March 2023

Revised: 28 April 2023

Accepted: 28 April 2023

Published: 4 May 2023



Copyright: © 2023 by the authors. Licensee MDPI, Basel, Switzerland. This article is an open access article distributed under the terms and conditions of the Creative Commons Attribution (CC BY) license (<https://creativecommons.org/licenses/by/4.0/>).

1. Introduction

The mantle is a specific microscopically inhomogeneous layer of a neutron star, where nuclear cluster shapes are essentially non-spherical. This layer was predicted for the first time in Refs. [1,2] by considering a set of symmetrical pasta-like nuclear shapes—cylinders, plates, and their inverse configurations—along with spherical nuclei and spherical holes. This set has become canonical and was considered in a large number of subsequent papers (e.g., [3–23]), and some papers suggested more complex structures based on numerical simulations [24–26]. In this paper, we limit ourselves to cylindrical nuclear shapes (both inverse and normal).

The mantle affects neutron star evolution (e.g., [27] for review), through its effect on the transport properties (e.g., [28–33]) and neutrino emissivity (e.g., [34–37]). However, in this paper, we concentrate on another aspect of mantle properties: elasticity. Indeed, each pasta-like layer of the mantle is similar to liquid crystal and can support shear stresses (see [38], for example). Its elastic properties can affect present-day observations (e.g., quasi-periodic oscillations, observed after magnetar flares [39–41] as well as constraints on quadrupole ellipticity supported by the crust [40]), and, as a part of the crust elasticity, can potentially affect the observations of the third generation of gravitational wave detectors (e.g., [42]; see, however, the critique in [43]).

The seminal work on the elastic properties of the mantle was made in Ref. [38]. Therein, the authors calculated elastic constants for cylindrical and planar nuclear shapes in the framework of a compressible liquid drop model (CLDM). Most of the results were obtained analytically, using some simplified assumptions. The elastic properties of the mantle were also studied using molecular dynamics [44] and relativistic-mean-field model [45]; special attention was paid to the problem of effective shear modulus in a realistic case in which non-spherical nuclei are not well ordered, considering global hydrodynamical scales of a star, i.e., the mantle has a “polycrystalline” structure [46].

In this paper, we elaborate on CLDM for the elasticity of the mantle. Specifically, we use our recent work [47], where we have demonstrated that shear deformation of a

neutron star crust induces quadrupole deformation for the initially spherical nuclei, and this effect reduces the effective shear modulus. Here, we generalize the approach of [47] for cylindrical pasta phases and consider transversal shear, i.e., shear deformations in the plane perpendicular to the symmetry axis of the cylinders. Regarding spherical nuclei, we demonstrate that the respective elastic constant (coefficient C in notations of [38]) can be analytically calculated within a simplified Wigner–Seitz approximation, and the result agrees well with accurate lattice-based calculations [38], if the same assumption (enforced circular shape of the cluster cross-section) is applied. As pointed out in [38], the shape of nuclear clusters can be affected by transversal shear. We take this effect into account analytically, allowing nuclear clusters to adjust their shape to minimize energy in response to the shear of the lattice. We demonstrate that shear deformation indeed enforces nuclei clusters to have elliptical cross-sections and, if one accounts for this effect, one obtains $\sim 25\%$ reduction of the respective elastic constant at the most relevant parameters. In Section 2, we present our formalism and derive the expression for transverse shear modulus for cylindrical clusters. In Section 3, we show our results and compare them with previous works. In Section 4, we present a summary of the results.

2. Formalism

Nuclear clusters in the mantle have a microscopical structure similar to that of liquid crystals resembling an intermediate state between solids and liquids in terms of elastic properties [38,44,46]. In what follows, we use terminology and the notation of Ref. [38]. For the considered cylindrical phase, three elastic constants B , C , and K_3 are generally required to describe shear deformations (the compression is described by a fourth constant, the bulk modulus, which can be easily calculated from the equation of state). The constant B characterizes the response to elongation along the cylindrical axis, accompanied by compression in the radial direction, K_3 is associated with bending, and C describes transverse shearing. In this paper, we limit ourselves to the elastic constant C .

To calculate the elastic constant C , we proceed in the same way as in [47]. First, we note that a straightforward consideration of deformation for a system of cylindrical clusters, ordered into a perfect static two-dimensional hexagonal lattice (as was carried out in [38]) is equivalent to the deformation of one unit cell with periodic boundary conditions. This is obvious because the whole crystal (for both undeformed and deformed states) can be presented as a set of periodic copies of the unit cell. Second, we replace a precise unit cell (regular hexagon) with a smoother figure—a cylinder with a circular cross-section with radius r_c —and apply shear deformation

$$x \rightarrow x(1 + \varepsilon) \quad (1)$$

$$y \rightarrow y/(1 + \varepsilon) \quad (2)$$

$$z \rightarrow z \quad (3)$$

for this cell. Here, the z axis is along the cylindrical axis and ε is an infinitesimally small strain parameter. As a result of this volume-conserving deformation, the approximate unit cell for the deformed state becomes a cylinder with an elliptical cross-section with semi-axes $r_c(1 + \varepsilon)$ and $r_c/(1 + \varepsilon)$ (see Figure 1). The high accuracy of the approach based on the approximate unit cell is confirmed below by comparison with the results of [38] (to do this, we provide an additional estimate of C , with an enforced circular shape of the cluster cross-sections, as was assumed in [38]).

By definition (see Equation (11) in [38]), for the specified deformation (Equations (1)–(3)), the energy density change is coupled with the elastic constant C by

$$\delta w = 2 C \varepsilon^2. \quad (4)$$

Thus, it is enough to calculate the energy density change δw to estimate C .

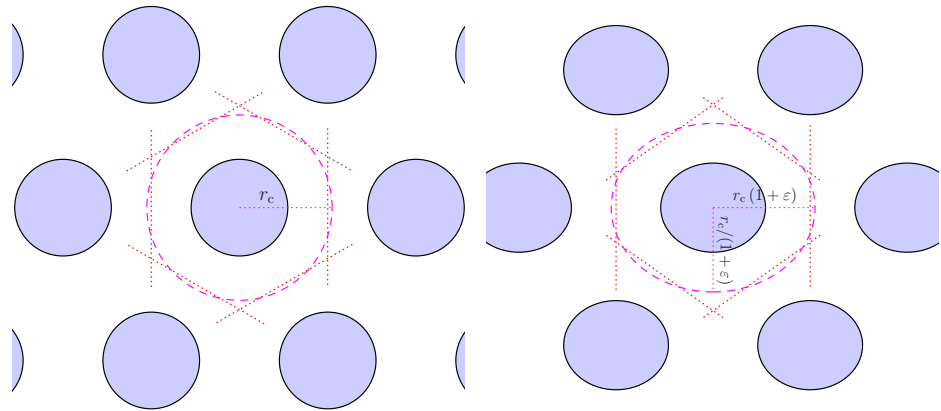


Figure 1. Transversal cross-section of the lattice of cylindrical clusters (filled regions) in the spaghetti phase before (**left** panel) and after (**right** panel) transversal shearing. Dotted lines represent the accurate hexagonal boundaries of the Wigner–Seitz cell, and dashed lines are the circular/elliptical approximations of the cell. The change in the cluster cross-section in response to the applied shear is schematically shown in the right panel.

To calculate the energy density in the deformed and undeformed states, we apply a compressible liquid drop model (CLDM) in the same way as in [48], i.e., we parametrize the surface parameters for a plain interface using the neutron chemical potential μ_n , taking into account neutron adsorption (adsorption of protons vanishes due to the choice of the reference frame; see supplementary material in [48] for details), but neglect curvature corrections. Below, we provide derivations for the non-inverted cylindrical phase,¹ i.e., we consider a cell with a neutron–proton cluster (with number densities n_{ni} and n_{pi}) located in a central part, surrounded by a neutron matter with number density n_{no} (see Figure 1). In comparison with [38], we allow the cluster cross-section in the x, y plane to respond to the applied shear. As long as we consider infinitesimal deformations, the cross-section in the deformed state can be treated as ellipsoidal with semi-axes $r_p(1 + \varepsilon_p)$ and $r_p/(1 + \varepsilon_p)$. Here, ε_p is an infinitesimal parameter, which allows us to adjust the cluster shape to minimize energy density. Below, we consider the case when the semi-axis $r_p(1 + \varepsilon_p)$ of the cluster cross-section lies along x . We have checked that it is this configuration, which corresponds to the minimal energy density within a more general treatment, that allows the cluster deformation to be oriented arbitrarily. Please note that the volume fraction, occupied by the cluster, depends neither on ε nor on ε_p , and can be written as $u \equiv (r_p/r_c)^2$. As usual, we assume the cell to be quasi-neutral, filled by degenerate electrons with uniform density in the whole cell. As a result, the energy density is

$$w = uw_b(n_{ni}, n_{pi}) + (1 - u)w_b(n_{no}, n_{po} = 0) + w_s + w_c + w_e(n_e). \quad (5)$$

Here, $w_b(n_n, n_p)$ is the bulk energy density of uniform nuclear matter at neutron and proton number densities n_n and n_p , and $w_e(n_e)$ is the energy density of degenerate electrons with the number density $n_e = u n_{pi}$. Finally, w_s is the energy density associated with the surface energy of the cluster, and w_c is the Coulomb energy density (averaged over the cell). These quantities are derived below.

As usual, within CLDM models, we assume that the internal parameters (n_{ni} , n_{pi} , n_{no} , r_c , r_p , ε_p) are adjusted to minimize the energy density at given external parameters. In the case of a deformed lattice, the external parameters are the baryon number density n_b and the shear parameter ε .

To derive the energy density associated with surface energy w_s , we remind the reader that the surface energy per unit area is $\sigma + \mu_n \nu_s$, where σ is the surface tension, and ν_s is the surface number density of the adsorbed neutrons (see [49,50], for example). The area

of the cylindrical cluster is given by the product of the cluster height $2H$ to the perimeter (circumference) of the cluster cross-section P . This allows the recording of the energy density, associated with surface energy, in the form

$$w_S = \frac{(\sigma + \mu_n \nu_S)P}{\pi r_c^2}. \quad (6)$$

As written above, we assume the cluster cross-section to be an ellipse with semi-axes $r_p(1 + \varepsilon_p)$ and $r_p/(1 + \varepsilon_p)$. Assuming $\varepsilon_p > 0$, the major semi-axis is $r_p(1 + \varepsilon_p)$ and

$$P = 4r_p(1 + \varepsilon_p) \int_0^{\pi/2} \sqrt{1 - k^2 \cos^2 t} dt = 4r_p(1 + \varepsilon_p)E(k^2), \quad (7)$$

where $E(k)$ is the complete elliptic integral of the second kind (see, for example, [51]) and $k = \sqrt{1 - 1/(1 + \varepsilon_p)^4}$ is the eccentricity of the cluster cross-section. Using the series for $E(k^2)$ (see, for example, equation (17.3.12) in [51]) or straightforwardly applying Equation (45) from [52], we obtain $P = 2\pi r_p \left(1 + 3\varepsilon_p^2/4 + O(\varepsilon_p^3)\right)$,² leading to the final expression for the surface energy density

$$w_S = \frac{2u(\sigma + \mu_n \nu_S)}{r_p} \left(1 + \frac{3}{4}\varepsilon_p^2\right). \quad (8)$$

It is easy to check that the same equation also holds for $\varepsilon_p < 0$ (for this aim, it is enough to repeat derivations in this passage, taking into account that the major semi-axis for $\varepsilon_p < 0$ is $r_p/(1 + \varepsilon_p)$, and thus eccentricity $k = \sqrt{1 - (1 + \varepsilon_p)^4}$).

Within CLDM, the calculation of the Coulomb energy density w_C reduces to the essentially electrostatic problem: the calculation of the energy of the neutral system composed of a positively uniformly charged cylinder (protons inside the cluster) inserted into a negatively charged cylinder (electrons). The Coulomb energy density can be written in the form

$$w_C = \frac{1}{2\pi r_c^2} \int \rho_p(\mathbf{r})\varphi_p(\mathbf{r})d^2\mathbf{r} + \frac{1}{2\pi r_c^2} \int \rho_e(\mathbf{r})\varphi_e(\mathbf{r})d^2\mathbf{r} + \frac{1}{\pi r_c^2} \int \rho_p(\mathbf{r})\varphi_e(\mathbf{r})d^2\mathbf{r}, \quad (9)$$

where the integrals are taken over vector \mathbf{r} in the x, y plane, $\varphi_p(\mathbf{r})$ and $\varphi_e(\mathbf{r})$ are electrostatic potentials, created by protons and electrons, respectively; $\rho_p(\mathbf{r})$ and $\rho_e(\mathbf{r})$ are charge densities of protons and electrons, respectively. When considering this electrostatic problem we assume $\rho_p(\mathbf{r}) = en_{pi}$ inside the internal cylinder (cluster) and outside the internal cylinder $\rho_p(\mathbf{r}) = 0$; similarly, $\rho_e(\mathbf{r}) = -en_e$ inside the external cylinder (cell) and $\rho_e(\mathbf{r}) = 0$ outside the external cylinder. Here, e is elementary charge.

To apply (9), it is sufficient to know electrostatic potential inside a uniformly charged (charge density ρ) cylinder with an elliptical cross-section (semi-axes a_x and a_y along x and y , respectively). This potential can be written as (e.g., [53]):

$$\phi = \pi\rho \left\{ 2a_x a_y \left[\ln\left(\frac{4H}{a_x + a_y}\right) + \frac{1}{2} \right] - \frac{2(a_y x^2 + a_x y^2)}{a_x + a_y} \right\}. \quad (10)$$

Here, $2H$ is the height of the cylinder, which is assumed to be large ($H \gg a_x$ and $H \gg a_y$).

Taking into account that the ellipticities of the cell and cluster are infinitesimally small, it is straightforward to write down

$$w_C = \frac{\pi}{2} u e^2 n_{pi}^2 r_p^2 \left[u - 1 - \ln(u) + (2u - 1)\varepsilon_p^2 - 2u\varepsilon_p\varepsilon + \varepsilon^2 \right] + \dots \quad (11)$$

where terms of the third and higher order in cluster and cell ellipticities are omitted. As it should be, H is canceled out in the final expression.

Now, it is easy to write down equations for internal variables by minimizing the energy density at fixed n_b and ε . As in the case of spherical nuclei, considered in [47], the majority of internal variables (n_{ni} , n_{pi} , n_{no} , r_c , r_p) can be derived at $\varepsilon = 0$ up to corrections of order of ε^2 ,³ and only $\varepsilon_p \propto \varepsilon$:

$$0 = \pi u e^2 n_{pi}^2 r_p^2 [(2u - 1)\varepsilon_p - u\varepsilon] + \frac{3\sigma u}{r_p} \varepsilon_p. \quad (12)$$

Equations for $\varepsilon = 0$ are well known (e.g., [48] in the case of spherical nuclei); their physical meaning is the chemical equilibrium within the cell, beta-equilibrium, pressure balance for the cluster, and the equation for the equilibrium size of the cell. The latter is often called virial theorem (see, for example, [1,2]), and it is the only equation that would be required below in the explicit form:

$$\frac{\sigma u}{r_p} = \frac{\pi}{2} \rho_p^2 r_p^2 u (u - 1 - \ln(u)). \quad (13)$$

Virial theorem allows the exclusion of σ , removing explicit dependence of the subsequent results on the nuclear physical model. Indeed, the bulk contributions to the total variation of energy are canceled out, and it can be written in the form

$$\delta w = \pi \rho_p^2 r_p^2 u \left[\frac{1}{2} \varepsilon^2 - u \varepsilon_p + \frac{7u - 5 - 3 \ln(u)}{4} \varepsilon_p^2 \right]. \quad (14)$$

In the case of $\varepsilon = 0$, considered in [6], it agrees with the sum of Equations (6)–(9) from that work. For $\varepsilon \neq 0$, the optimal cluster-deformation parameter, given by the solution of Equation (12), is

$$\varepsilon_p = \frac{2u}{7u - 5 - 3 \ln(u)} \varepsilon. \quad (15)$$

Substituting (15) into (14) and using (4) we come to the final expression for the elastic constant for the transverse shear:

$$C = \frac{\pi \rho_p^2 r_p^2 u}{4} \left(1 - \frac{2u^2}{7u - 5 - 3 \ln(u)} \right). \quad (16)$$

It is worth stressing that the $\partial^2 \delta w / \partial \varepsilon_p^2$, calculated at the optimal value of ε_p , is positive for an arbitrary filling factor. Therefore, the clusters can indeed adjust their shape and become stable with respect to additional infinitesimal deformations. The stability of cylinders in an undeformed lattice ($\varepsilon = 0$) was proven in Ref. [6]. A similar result was obtained by the authors in [54], according to which the spherical nuclei in the crust are stable with respect to infinitesimal quadrupole deformations, and thus transition from the crust to the mantle is not associated with the absolute instability of spherical nuclei.

To compare our approach with the results of the authors in [38]; we also consider the approximation of the enforced circular shape of cluster cross-section ($\varepsilon_p = 0$, not adjusted to the deformation). It leads to a simplified estimate of transverse shear modulus

$$C^{sp} = \frac{\pi \rho_p^2 r_p^2 u}{4}. \quad (17)$$

3. Results

In Figure 2, we demonstrate the ratio $\varepsilon_p / \varepsilon$, given by Equation (15), as a function of filling factor u (solid line). For a typical filling factor of the cylindrical phases, $u \approx 0.2 \div 0.3$ (e.g., [2,13]), the cluster deformation evolves from $\varepsilon_p \approx 0.3\varepsilon$ to the value, which is close to ε ($\varepsilon_p \approx 0.85\varepsilon$). For comparison, the dotted line indicates a similar ratio for spherical clusters, which was obtained by the authors in [47]. One can see that this ratio depends on the shape of the clusters. In particular, for $u \approx 0.2$, which is typical for the transition from spherical

to cylindrical clusters (e.g., [13]), the shape of spherical clusters is approximately two times more sensitive to the shear deformations than the shape of cylindrical clusters.

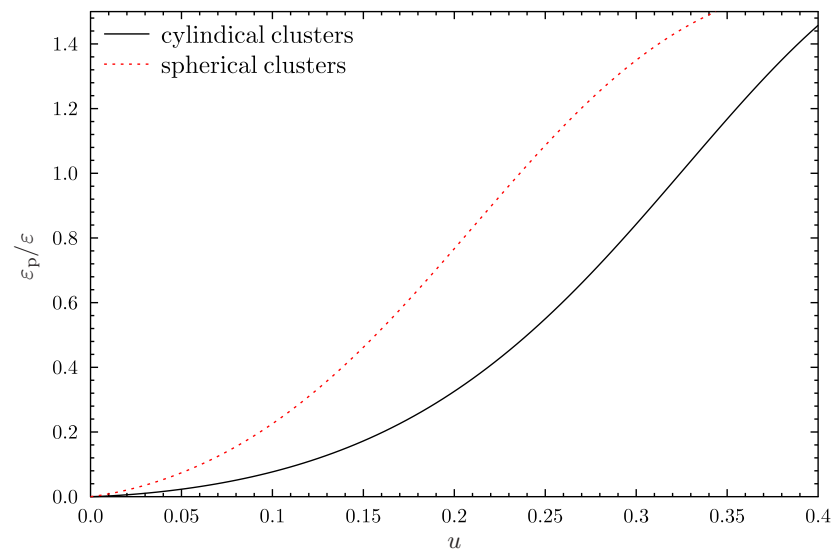


Figure 2. The ratio of cluster-deformation parameter ε_p to the shear parameter ε as a function of the filling factor u . The solid line is for cylindrical clusters (this work); the dotted line is for spherical clusters (Ref. [47]).

To compare our results with previous works, in Figure 3, we demonstrate the transverse shear modulus, normalized to the Coulomb energy density in the non-deformed state w_C^0 (see Equation (11) for $\varepsilon = \varepsilon_p = 0$) as a function of filling factor u . The solid line represents our final expression (16), while the long-dashed line is for Equation (17) ignoring the change in the cross-section shape. The latter agrees well with the fit provided in Ref. [38] (see short dashes), which was based on calculations with the accurate treatment of hexagonal (honeycomb) lattice, but with fixed circular cross-section of the cylindrical clusters. Please note that the authors of [38] fitted their numerical results for reasonable filling factor $u \sim 0.2 \div 0.3$ (e.g., [2,13]).

Recently, the authors of [45] analyzed the elastic properties of nuclear pasta in a full three-dimensional geometry. Their calculations were performed within the Thomas–Fermi approach based on the relativistic-mean-field model, and thus should include a change in the cluster cross-section shape with increasing deformation. The fit for the transversal shear modulus suggested in [45] is shown by a dotted line in Figure 3. It predicts a much smaller suppression of C than our result (16).

However, we should note that rather large deformations (from a hexagonal to a simple lattice) were applied to extract C in [45]. Specifically, the authors of [45] performed numerical simulations for a wide set of deformation parameters at a fixed baryon number density and fitted the results by their Equation (13). As a result, their Equation (13) reproduces well the deformation energy for the whole deformation path from one hexagonal to another hexagonal lattice via simple lattice (see Figure 3 in [45]). However, it has only one fitted parameter (elastic constant, which we denote as C_{13}). It seems to be most affected by the energy difference between hexagonal and simple lattices (which is indeed perfectly reproduced, according to Figure 3 in Ref. [45]), but not to the details of infinitesimal deformations of a hexagonal lattice.

Let us note that there should be no elliptical deformation of the cluster cross-sections for both simple and hexagonal lattices due to symmetry. Therefore, the energy difference between these lattices can be reasonably estimated assuming a circular cluster shape. As a result, the effects of the elliptical deformation of a cluster cross-section can be suppressed in C_{13} , overestimating the elastic constant C . Indeed, our attempt to directly fit numerical data, shown in Figure 3 of [45] for small transversal shearing, leads to $C \sim 0.8C_{13}$, i.e., 20%

smaller than the estimate of the shear modulus suggested in Ref. [45] (the red line at the same plot). Thus, we expect that the actual transversal shear modulus for infinitesimal deformation of a hexagonal lattice can be smaller than that given by the final fit presented in [45] being closer to our Equation (16).

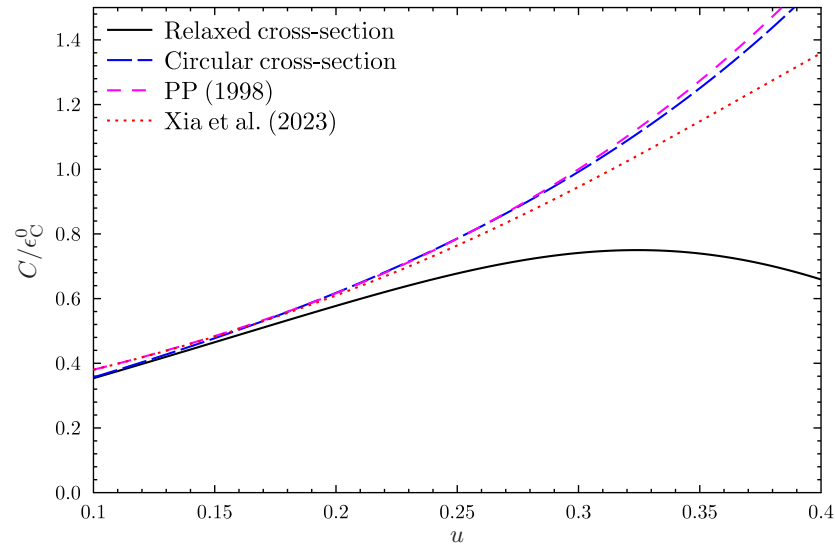


Figure 3. Transversal shear modulus C for the “spaghetti” phase of a neutron star mantle as a function of filling factor. The solid and long-dashed lines are our results, with optimized (Equation (16)) and circular (Equation (17)) shapes of cluster cross-section, respectively. Short dashes represent the fit from the authors in [38], while the dotted line corresponds to the fit from the authors in [45].

Unfortunately, we cannot check this hypothesis directly because the filling factor for the baryon number density $n_b = 0.06 \text{ fm}^{-3}$, analyzed in their Figure 3, is not quoted in Ref. [45]. However, we can estimate the filling factor using figures in Ref. [13]. Indeed, Figure 3 in [45] is plotted for the slope of the symmetry energy $L = 41.34 \text{ MeV}$. Therefore, according to Figure 4 of [13], $n_b = 0.06 \text{ fm}^{-3}$ should be close to the transition from spherical to cylindrical clusters, and, according to Figure 3 of the same work it should correspond to $u \approx 0.2$. In this case, our Equation (16) predicts C to be suppressed by $\sim 6.5\%$ with respect to results for a fixed (circular) cluster cross-section, which almost coincides with C_{13} for $u \approx 0.2$. Formally, it disagrees with the estimate $C \sim 0.8C_{13}$ mentioned above, and suggests that our Equation (16), in fact, overestimates C . However, due to the qualitative nature of estimates in this passage, we prefer to treat this conclusion as very tentative.

As discussed in [19], the actual shape of nuclear clusters at a given number density is rather model-dependent, even if the nucleon interaction model is fixed. For example, for Skyrme Lyon nucleon interaction model SLy4 [55], which was analyzed by the authors in [19], the cylindrical clusters are the most energetically favorable at baryon number density $0.056 \text{ fm}^{-3} \lesssim n_b \lesssim 0.075 \text{ fm}^{-3}$, if energy density is calculated within ETF approach, and CLDM predicts it to be favorable only in a narrow region $0.074 \text{ fm}^{-3} \lesssim n_b \lesssim 0.076 \text{ fm}^{-3}$. Thus, to illustrate our results in physical units (see Figure 4), we use a rather wide n_b region; following [19], we applied the SLy4 nucleon interaction model for numerical estimates. As in Figure 3, the solid line represents our final expression (16), while the long-dashed line is for Equation (17), which ignores the change in the cross-section shape. Short dashes correspond to the fit provided in Ref. [38], while the dotted line is for the fit provided in Ref. [45]. Please note that both fits present the ratio of C to the Coulomb energy density, and, in our calculations, we apply CLDM [48] to calculate the latter. The upper panel demonstrates the cluster volume fraction u . As discussed in [50], the latter quantity can be estimated in so-called bulk approximation, being weakly dependent on the shape of the clusters and the applied approach (ETF or CLDM).

For the whole indicated density region, our results predict the transversal shear modulus C to be lower than according to fits from the authors in [38,45]. For low baryon number density $n_b \lesssim 0.065 \text{ fm}^{-3}$, it is associated with low volume fraction $u \lesssim 0.15$, where the fit provided in Ref. [45] almost coincides with that of [38]. However, the latter overestimates the original numerical calculations of that work for $u \lesssim 0.15$ (see Figure 2 in [38]). Thus, we expect that our Equation (16) is, in fact, more accurate than the fits provided in Refs. [38,45], at least for low-density regions. The larger the density, the larger the effect of the relaxation of the cluster cross-section. For $n_b \gtrsim 0.07 \text{ fm}^{-3}$, it leads to a decrease of C with an increase of n_b , despite the fact that C^{SP} , calculated neglecting this effect, increases with an increase of n_b .

For comparison, in Figure 4 we also plotted the effective shear modulus μ for inner crust matter, assuming a spherical shape of the clusters [47]. A thin solid line was calculated, taking into account the relaxation of the cluster shape, while a dashed line neglects this effect. One can see that the effective shear modulus μ is lower than the transversal shear modulus C for the same baryon number density. According to this principle, it can lead to a jump in elastic properties at the inner crust/mantle boundary. However, one should take in mind that it is rather tricky to estimate the effective shear modulus of “polycrystalline” pasta phases (see [46] for discussion). In particular, it can vanish if pasta elements are spatially uniform (because the elastic constant, responsible for deformation along the pasta structure, is zero in a strictly uniform case). Therefore, we refrain from speculation on possible observational consequences of the difference between C and μ .

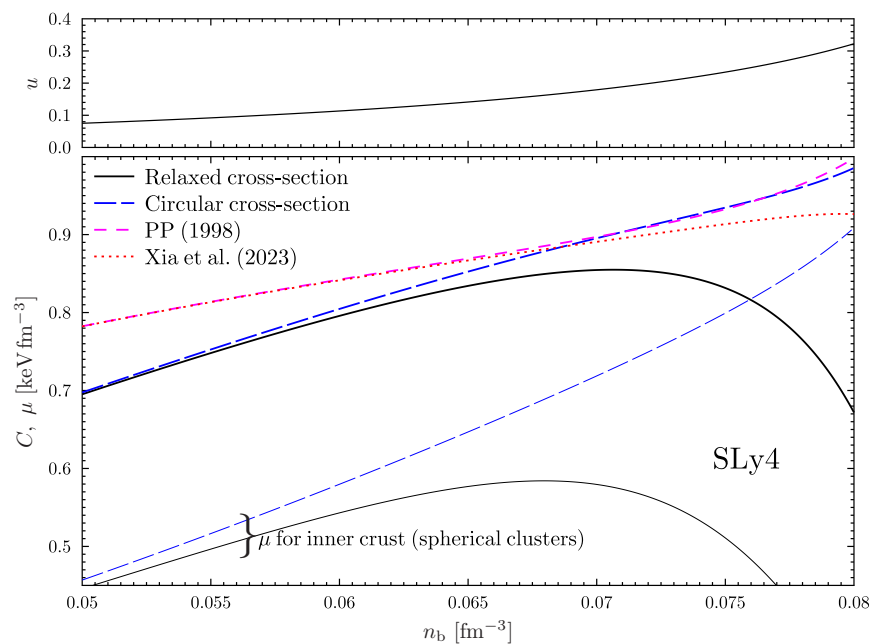


Figure 4. Transversal shear modulus C for the ‘spaghetti’ phase of the neutron star mantle in physical units as a function of baryon number density n_b . As in figure 3, the solid and long-dashed lines are our results, calculated with optimized (Equation (16)) and circular (Equation (17)) shapes of cluster cross-section, respectively. Short dashes represent the fit [38]; the dotted line corresponds to the fit [45]. In addition, thin lines represent the effective shear modulus for spherical nuclear clusters, as calculated by the authors in [47]. Specifically, a thin solid line accounts for nuclei deformation (Equation (9) in [47]), while a thin dashed line neglects this effect (Equation (6) in [47]). The upper panel represents the cluster volume fraction u . The SLy4 nucleon interaction model [55] was used to calculate bulk energy contribution; the surface tension was calculated according to the fit of the fourth-order ETF calculations for the SLy4 model, provided by N.N. Shchepochin (the same fit was used in [19]).

4. Summary and Discussion

We analytically derived the transversal shear modulus C for the spaghetti phase of nuclear pasta (see Equation (16); the result for the inverted phase can be obtained using note 1). Following the predictions of the authors in [38], we demonstrated that shear deformation affects the shape of nuclear clusters (the transversal cluster cross-section becomes elliptical) and we took this effect into account. It is worth noting that our final expression for C is explicitly independent of the parameters of inter-nucleon interaction.

Our results agree with the well-known fit [38], if one neglects cluster deformation, as was carried out in Ref. [38]. Accounting for cluster deformation reduces C (for example, C is reduced by 25% at the filling factor $u \sim 0.3$). However, the practical fit, suggested in a recent paper [45] on the base of numerical simulations in fully three-dimensional geometry, predicts a much smaller reduction of C than in [38]. As we argued in Section 3, this difference can be associated with the numerical procedure in [45]. Specifically, the practical expression in [45], suggests a parameter for their Equation (13), which allows the description of deformation energy for strong transversal deformations, but is not, however, very precise for smaller deformations.

Finally, we should remind the reader that our approach is not exact by construction, being based on two simplifications: (1) we neglect curvature corrections to surface tension; (2) we apply ellipsoidal approximation for the cell cross-section. Both of these approximations can affect C , and we plan to check their importance in subsequent studies.

Author Contributions: Derivations, N.A.Z.; formulation of the problem, supervision, A.I.C. All authors have read and agreed with the published version of the manuscript.

Funding: This research received no external funding.

Data Availability Statement: Not applicable.

Acknowledgments: We thank Nikolai N. Shchepochin for providing us with the fit of the fourth-order ETF calculations of the surface tension for the SLy4 model.

Conflicts of Interest: The authors declare no conflict of interest.

Abbreviations

The following abbreviations are used in this manuscript:

CLDM	Compressible liquid drop model
ETF	Extended Thomas–Fermi

Notes

- ¹ Derivations for the inverted phase can be performed straightforwardly by substituting $u \rightarrow 1 - u$, and treating r_p as the linear radius of the neutron phase, located in the center.
- ² Note that terms up to k^4 should be included to obtain this expression.
- ³ Thanks to the minimization procedure over internal variables, corrections in the order of ε^2 contribute to the energy at the order of ε^4 , and thus can be neglected

References

1. Ravenhall, D.G.; Pethick, C.J.; Wilson, J.R. Structure of Matter below Nuclear Saturation Density. *Phys. Rev. Lett.* **1983**, *50*, 2066–2069. [\[CrossRef\]](#)
2. Hashimoto, M.; Seki, H.; Yamada, M. Shape of nuclei in the crust of a neutron star. *Prog. Theor. Phys.* **1984**, *71*, 320–326. [\[CrossRef\]](#)
3. Lorenz, C.P.; Ravenhall, D.G.; Pethick, C.J. Neutron star crusts. *Phys. Rev. Lett.* **1993**, *70*, 379–382. [\[CrossRef\]](#) [\[PubMed\]](#)
4. Oyamatsu, K. Nuclear shapes in the inner crust of a neutron star. *Nucl. Phys. A* **1993**, *561*, 431–452. [\[CrossRef\]](#)
5. Douchin, F.; Haensel, P.; Meyer, J. Nuclear surface and curvature properties for SLy Skyrme forces and nuclei in the inner neutron-star crust. *Nucl. Phys. A* **2000**, *665*, 419–446. [\[CrossRef\]](#)
6. Iida, K.; Watanabe, G.; Sato, K. Formation of Nuclear “Pasta” in Cold Neutron Star Matter. *Prog. Theor. Phys.* **2001**, *106*, 551–559. [\[CrossRef\]](#)
7. Nakazato, K.; Iida, K.; Oyamatsu, K. Curvature effect on nuclear “pasta”: Is it helpful for gyroid appearance? *Phys. Rev. C* **2011**, *83*, 065811. [\[CrossRef\]](#)

8. Newton, W.G.; Gearheart, M.; Li, B.A. A Survey of the Parameter Space of the Compressible Liquid Drop Model as Applied to the Neutron Star Inner Crust. *Astrophys. J. Suppl. Ser.* **2013**, *204*, 9. [[CrossRef](#)]
9. Sharma, B.K.; Centelles, M.; Viñas, X.; Baldo, M.; Burgio, G.F. Unified equation of state for neutron stars on a microscopic basis. *Astron. Astrophys.* **2015**, *584*, A103. [[CrossRef](#)]
10. Schuettrumpf, B.; Nazarewicz, W. Twist-averaged boundary conditions for nuclear pasta Hartree-Fock calculations. *Phys. Rev. C* **2015**, *92*, 045806. [[CrossRef](#)]
11. Fattoyev, F.J.; Horowitz, C.J.; Schuettrumpf, B. Quantum nuclear pasta and nuclear symmetry energy. *Phys. Rev. C* **2017**, *95*, 055804. [[CrossRef](#)]
12. Pearson, J.M.; Chamel, N.; Potekhin, A.Y. Unified equations of state for cold nonaccreting neutron stars with Brussels-Montreal functionals. II. Pasta phases in semiclassical approximation. *Phys. Rev. C* **2020**, *101*, 015802. [[CrossRef](#)]
13. Oyamatsu, K.; Iida, K.; Sotani, H. Systematic study of pasta nuclei in neutron stars with families of the empirical nuclear equations of state. *J. Phys. Conf. Ser.* **2020**, *1643*, 012059. [[CrossRef](#)]
14. Xia, C.J.; Maruyama, T.; Yasutake, N.; Tatsumi, T.; Zhang, Y.X. Nuclear pasta structures and symmetry energy. *Phys. Rev. C* **2021**, *103*, 055812. [[CrossRef](#)]
15. Ji, F.; Hu, J.; Shen, H. Nuclear pasta and symmetry energy in the relativistic point-coupling model. *Phys. Rev. C* **2021**, *103*, 055802. [[CrossRef](#)]
16. Dinh Thi, H.; Carreau, T.; Fantina, A.F.; Gulminelli, F. Uncertainties in the pasta-phase properties of catalysed neutron stars. *Astron. Astrophys.* **2021**, *654*, A114. [[CrossRef](#)]
17. Dinh Thi, H.; Fantina, A.F.; Gulminelli, F. The effect of the energy functional on the pasta-phase properties of catalysed neutron stars. *Eur. Phys. J. A* **2021**, *57*, 296. [[CrossRef](#)]
18. Pearson, J.M.; Chamel, N. Unified equations of state for cold nonaccreting neutron stars with Brussels-Montreal functionals. III. Inclusion of microscopic corrections to pasta phases. *Phys. Rev. C* **2022**, *105*, 015803. [[CrossRef](#)]
19. Shchepochin, N.N.; Zemlyakov, N.A.; Chugunov, A.I.; Gusakov, M.E. Pasta Phases in Neutron Star Mantle: Extended Thomas–Fermi vs. Compressible Liquid Drop Approaches. *Universe* **2022**, *8*, 582. [[CrossRef](#)]
20. Parmar, V.; Das, H.C.; Kumar, A.; Kumar, A.; Sharma, M.K.; Arumugam, P.; Patra, S.K. Pasta properties of the neutron star within effective relativistic mean-field model. *Phys. Rev. D* **2022**, *106*, 023031. [[CrossRef](#)]
21. Chamel, N.; Pearson, J.M.; Shchepochin, N. Is there pasta in neutron stars? *Eur. Phys. J. Web Conf.* **2022**, *274*, 07013. [[CrossRef](#)]
22. Dinh Thi, H.; Fantina, A.F.; Gulminelli, F. Properties of pasta phases in catalyzed neutron stars. *arXiv* **2022**, arXiv:2206.07969.
23. Pelicer, M.R.; Menezes, D.P.; Dutra, M.; Lourenço, O. Do short range correlations inhibit the appearance of the nuclear pasta? *arXiv* **2022**, arXiv:2211.14002.
24. Berry, D.K.; Caplan, M.E.; Horowitz, C.J.; Huber, G.; Schneider, A.S. “Parking-garage” structures in nuclear astrophysics and cellular biophysics. *Phys. Rev. C* **2016**, *94*, 055801. [[CrossRef](#)]
25. Schneider, A.S.; Berry, D.K.; Briggs, C.M.; Caplan, M.E.; Horowitz, C.J. Nuclear “waffles”. *Phys. Rev. C* **2014**, *90*, 055805. [[CrossRef](#)]
26. Newton, W.G.; Cantu, S.; Wang, S.; Stinson, A.; Kaltenborn, M.A.; Stone, J.R. Glassy quantum nuclear pasta in neutron star crusts. *Phys. Rev. C* **2022**, *105*, 025806. [[CrossRef](#)]
27. Caplan, M.E.; Horowitz, C.J. Colloquium: Astromaterial science and nuclear pasta. *Rev. Mod. Phys.* **2017**, *89*, 041002. [[CrossRef](#)]
28. Horowitz, C.J.; Berry, D.K. Shear viscosity and thermal conductivity of nuclear “pasta”. *Phys. Rev. C* **2008**, *78*, 035806. [[CrossRef](#)]
29. Yakovlev, D.G. Electron transport through nuclear pasta in magnetized neutron stars. *Mon. Not. R. Astron. Soc.* **2015**, *453*, 581–590. [[CrossRef](#)]
30. Schmitt, A.; Shternin, P. Reaction Rates and Transport in Neutron Stars. In *The Physics and Astrophysics of Neutron Stars*; Rezzolla, L., Pizzochero, P., Jones, D.I., Rea, N., Vidaña, I., Eds.; Springer International Publishing: Cham, Switzerland, 2018; pp. 455–574. [[CrossRef](#)]
31. Yakovlev, D.G.; Gusakov, M.E.; Haensel, P. Bulk viscosity in a neutron star mantle. *Mon. Not. R. Astron. Soc.* **2018**, *481*, 4924–4930. [[CrossRef](#)]
32. Nandi, R.; Schramm, S. Transport Properties of the Nuclear Pasta Phase with Quantum Molecular Dynamics. *Astrophys. J.* **2018**, *852*, 135. [[CrossRef](#)]
33. Pelicer, M.R.; Antonelli, M.; Menezes, D.P.; Gulminelli, F. Anisotropic electron transport in the nuclear pasta phase. *Mon. Not. R. Astron. Soc.* **2023**, *521*, 743–759. [[CrossRef](#)]
34. Gusakov, M.E.; Yakovlev, D.G.; Haensel, P.; Gnedin, O.Y. Direct Urca process in a neutron star mantle. *Astron. Astrophys.* **2004**, *421*, 1143–1148. [[CrossRef](#)]
35. Alloy, M.D.; Menezes, D.P. Nuclear “pasta phase” and its consequences on neutrino opacities. *Phys. Rev. C* **2011**, *83*, 035803. [[CrossRef](#)]
36. Schuettrumpf, B.; Martínez-Pinedo, G.; Reinhard, P.G. Survey of nuclear pasta in the intermediate-density regime: Structure functions for neutrino scattering. *Phys. Rev. C* **2020**, *101*, 055804. [[CrossRef](#)]
37. Lin, Z.; Caplan, M.E.; Horowitz, C.J.; Lunardini, C. Fast neutrino cooling of nuclear pasta in neutron stars: Molecular dynamics simulations. *Phys. Rev. C* **2020**, *102*, 045801. [[CrossRef](#)]
38. Pethick, C.; Potekhin, A. Liquid crystals in the mantles of neutron stars. *Phys. Lett. B* **1998**, *427*, 7–12. [[CrossRef](#)]

39. Sotani, H. Constraints on pasta structure of neutron stars from oscillations in giant flares. *Mon. Not. R. Astron. Soc.* **2011**, *417*, L70–L73. [\[CrossRef\]](#)
40. Gearheart, M.; Newton, W.G.; Hooker, J.; Li, B.A. Upper limits on the observational effects of nuclear pasta in neutron stars. *Mon. Not. R. Astron. Soc.* **2011**, *418*, 2343–2349. [\[CrossRef\]](#)
41. Sotani, H. Crustal torsional oscillations inside the deeper pasta structures. *Astron. Nachrichten* **2019**, *340*, 920–923. [\[CrossRef\]](#)
42. Biswas, B.; Nandi, R.; Char, P.; Bose, S. Role of crustal physics in the tidal deformation of a neutron star. *Phys. Rev. D* **2019**, *100*, 044056. [\[CrossRef\]](#)
43. Gittins, F.; Andersson, N.; Pereira, J.P. Tidal deformations of neutron stars with elastic crusts. *Phys. Rev. D* **2020**, *101*, 103025. [\[CrossRef\]](#)
44. Caplan, M.E.; Schneider, A.S.; Horowitz, C.J. Elasticity of Nuclear Pasta. *Phys. Rev. Lett.* **2018**, *121*, 132701. [\[CrossRef\]](#)
45. Xia, C.J.; Maruyama, T.; Yasutake, N.; Tatsumi, T.; Zhang, Y.X. Elastic properties of nuclear pasta in a fully three-dimensional geometry. *Phys. Lett. B* **2023**, *839*, 137769. [\[CrossRef\]](#)
46. Pethick, C.J.; Zhang, Z.W.; Kobyakov, D.N. Elastic properties of phases with nonspherical nuclei in dense matter. *Phys. Rev. C* **2020**, *101*, 055802. [\[CrossRef\]](#)
47. Zemlyakov, N.A.; Chugunov, A.I. Neutron star inner crust: Reduction of shear modulus by nuclei finite size effect. *Mon. Not. R. Astron. Soc.* **2023**, *518*, 3813–3819. [\[CrossRef\]](#)
48. Gusakov, M.E.; Chugunov, A.I. Thermodynamically Consistent Equation of State for an Accreted Neutron Star Crust. *Phys. Rev. Lett.* **2020**, *124*, 191101. [\[CrossRef\]](#)
49. Lattimer, J.M.; Pethick, C.J.; Ravenhall, D.G.; Lamb, D.Q. Physical properties of hot, dense matter: The general case. *Nucl. Phys. A* **1985**, *432*, 646–742. [\[CrossRef\]](#)
50. Haensel, P.; Potekhin, A.Y.; Yakovlev, D.G. *Neutron Stars 1: Equation of State and Structure*; Springer: New York, NY, USA, 2007; Volume 326. [\[CrossRef\]](#)
51. Abramowitz, M.; Stegun, I.A. *Handbook of Mathematical Functions with Formulas, Graphs, and Mathematical Tables*; U.S. Government Printing Office: Washington, DC, USA, 1972.
52. Ramanujan, S. Modular Equations and Approximations to π . *Quart. J. Pure App. Math.* **1914**, *45*, 350–372.
53. Kondratyev, B.P. *Potential Theory. New Methods and Problems with Solutions*; Mir: Moscow, Russia, 2007. (In Russian)
54. Zemlyakov, N.A.; Chugunov, A.I. Stability of Spherical Nuclei in the Inner Crust of Neutron Stars. *Particles* **2022**, *5*, 225–234. [\[CrossRef\]](#)
55. Chabanat, E.; Bonche, P.; Haensel, P.; Meyer, J.; Schaeffer, R. A Skyrme parametrization from subnuclear to neutron star densities. *Nucl. Phys. A* **1997**, *627*, 710–746. [\[CrossRef\]](#)

Disclaimer/Publisher’s Note: The statements, opinions and data contained in all publications are solely those of the individual author(s) and contributor(s) and not of MDPI and/or the editor(s). MDPI and/or the editor(s) disclaim responsibility for any injury to people or property resulting from any ideas, methods, instructions or products referred to in the content.